DOI: 10.19884/j.1672-5220.202503004

Synthesis and Application of Rosin-Based Polyoxyethylene Ether Non-Ionic Gemini Surfactant

HAN Zhaoqiang[1], ZHANG Ruifeng[1], ZHANG Rui[1], WANG Bijia[1], JI Bolin[1], XU Hong[1], MAO Zhiping[1,2*], ZHONG Yi[1,3*]

1. Key Laboratory of Sustainable Low-carbon Technologies for Textile Dyeing and Finishing, Ministry of Education, College of Chemistry and Chemical Engineering, Innovation Center for Textile Science and Technology, Donghua University, Shanghai 201620, China
2. National Manufacturing Innovation Center of Advanced Dyeing and Finishing Technology, Shandong Zhongkang Guochuang Research Institute of Advanced Dyeing and Finishing Technology Co., Ltd., Tai'an 271000, China
3. College of Fashion and Textiles, Xinjiang Production & Construction Corps Key Laboratory of Modern Textile Materials and Technology, Tarim University, Alaer 843300, China

Abstract: In this research, novel rosin-based non-ionic Gemini surfactants (RNGSs) were synthesized from rosin derivatives, dehydroabietic acid (DAA) and dehydroabietylamine (DHAA), via addition and alkylation reactions. The structures of the synthesized surfactants were characterized by Fourier transform infrared (FTIR) spectroscopy and proton nuclear magnetic resonance (^{1}H NMR) spectroscopy. The surface activity, aggregation property, and foaming property of RNGSs in aqueous solution were investigated by surface tension measurement and dynamic light scattering (DLS). Furthermore, the cloud point was investigated to evaluate the upper temperature limit for practical application of the surfactants. To evaluate the potential of RNGSs for enhanced oil recovery (EOR), their interfacial tension (IFT), static adsorption capacity, salt tolerance, and emulsion stability were examined. The lowest critical micelle concentration (CMC) of RNGSs was 8.51×10^{-6} mol/L, lower than that of the commonly used non-ionic surfactant OP-10 (1.29×10^{-4} mol/L). The cloud point of RNGSs reached 72.6 ℃. Furthermore, the tolerance to NaCl and $CaCl_2$ was determined to be 300 and 10 g/L, respectively. The findings indicate that the synthesized surfactants possess the potential for application in EOR.

Keywords: non-ionic Gemini surfactant; rosin derivative; enhanced oil recovery

CLC number: TQ423.2 **Document code**: A

Article ID: 1672-5220(2026)04-0013-13

0 Introduction

Natural raw materials, such as cashew nut phenol and saponin, have attracted considerable attention for surfactant production due to their compatibility with the environment and degradation under natural or physiological conditions. China's forest industry is characterized by a wealth of resources[1] and is responsible for the largest annual production of rosin. Rosin is an abundant, renewable natural resource[2] derived from pine oleoresin, with abietic acid[3] as its major component. Abietic acid contains a carboxyl group and a conjugated double bond, and therefore can be easily modified[4]. The molecule of abietic acid is composed of a large, rigid tricyclic hydrophenanthrene structure, which is extremely hydrophobic[5]. Thus, rosin represents an ideal raw material for the synthesis of green surfactants[6-7].

Gemini surfactants consist of two hydrophobic chains and two hydrophilic head groups[8-10], connected by flexible or rigid spacer groups, which endow them with a unique amphiphilic molecular architecture[11]. In addition, as a new generation of surfactants, Gemini surfactants have extremely low critical micelle concentration (CMC) and superior wetting performance[12-14]. Several studies have focused on rosin and dehydrogenated rosin-based Gemini surfactants. Tan et al.[15] and Pan et al.[16] synthesized rosin-based quaternary ammonium Gemini surfactants. Xu et al.[17] developed a series of novel rosin-based bis-quaternary ammonium salts. Yan et al.[18] prepared a series of polymeric surfactants, polyacrylic acid rosin polyethylene glycol esters, from rosin. However, few studies have reported the synthesis of Gemini surfactants via alkylation of the aromatic hydrogen on dehydroabietic acid polyoxyethylene ether to link two such molecular units. This research presents a novel strategy to synthesize structurally distinct Gemini surfactants via alkylation of

Received date: 2025-03-05

Foundation item: Science and Technology Plan Project of XPCC, China (No. 2024AB060)

* Correspondence should be addressed to ZHONG Yi, email: zhongyi@dhu.edu.cn; MAO Zhiping, email: zhpmao@dhu.edu.cn

Citation: Han Z Q, Zhang R F, Zhang R, et al. Synthesis and application of rosin-based polyoxyethylene ether non-ionic Gemini surfactant[J]. *Journal of Donghua University (English Edition)*, 2026, 43(4): 13-25.

the aromatic hydrogen on the rosin skeleton, thereby filling this research gap and providing new insights into rosin-based Gemini surfactants.

In this research, rosin-based non-ionic Gemini surfactants were synthesized from rosin derivatives, dehydroabietic acid (DAA) and dehydroabietylamine (DHAA), via addition and alkylation reactions. The structure of the synthesized surfactants contains two rosin backbones, which significantly affect the CMC of the surfactants. The increased hydrophobic segments enhance intermolecular interactions, promoting rapid micellization and consequently lowering the CMC. The CMC of the synthesized surfactants is as low as 8.51×10^{-6} mol/L, which is lower than that of previously reported rosin-based surfactants[1, 19] and rosin-based Gemini surfactants[16, 20-22]. For example, the CMC of the rosin-based surfactant synthesized in Ref. [19] is 6.12×10^{-4} mol/L, while the CMC of the rosin-based Gemini surfactant synthesized in Ref. [22] is 7.8×10^{-5} mol/L. In addition, the salt tolerance of the surfactants synthesized in this study is superior to that of some previously reported oil-displacement agents[23-26]. For example, the alkyl polyether benzyl sulfonate surfactant reported by Bao et al.[24] showed salt tolerances of 180.0 and 7.2 g/L for NaCl and $CaCl_2$, respectively. To evaluate their potential for oilfield applications, the synthesized surfactants were assessed for their ability to reduce oil-water interfacial tension (IFT), emulsify crude oil, and withstand high salinity. Kerosene was used as the oil phase, and the temperature was set at 45 ℃, which corresponds to the reservoir temperature of the Daqing Oilfield.

1 Materials and Methods

1.1 Materials

DAA, paraformaldehyde, and kerosene were purchased from Shanghai Macklin Biochemical Co., Ltd., China. DHAA, ethyl acetate, and OP-10 were purchased from Shanghai Titan Scientific Co., Ltd., China. Sulfuric acid and sodium hydroxide were purchased from Sinopharm Chemical Reagent Co., Ltd., China. DAA and DHAA were subjected to ethoxylation modification by a commercial supplier to obtain dehydroabietic acid polyoxyethylene ether (DAA-EO_n, n= 9, 10) and dehydroabietylamine polyoxyethylene ether (DHAA-EO_n, n=10).

1.2 Synthesis

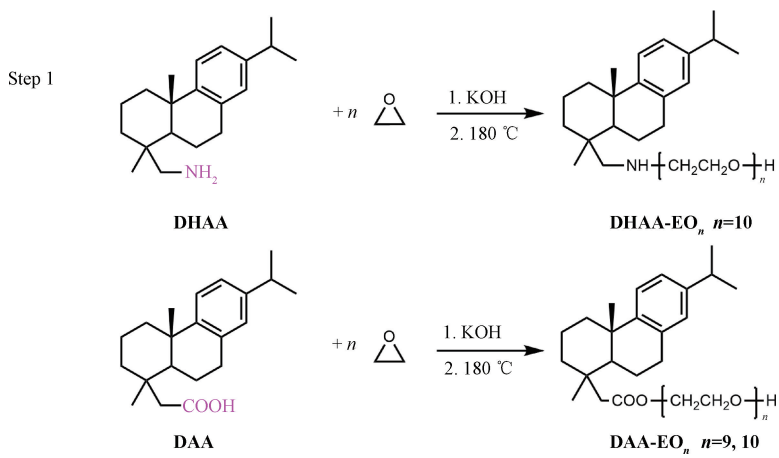
The synthetic procedures for Gemini dehydroabietic acid polyoxyethylene ether (G-DAA-EO_9 and G-DAA-EO_{10}), and Gemini dehydroabietylamine polyoxyethylene ether (G-DHAA-EO_{10}) are shown in Fig. 1. Since the synthetic routes for G-DHAA-EO_{10} and G-DAA-EO_n (n=9, 10) are similar, the synthesis of G-DHAA-EO_{10} is described here as a representative example. The structures of the synthesized Gemini surfactants were confirmed by Fourier transform infrared (FTIR) spectroscopy and proton nuclear magnetic resonance (^{1}H NMR) spectroscopy.

1.2.1 Synthesis of DHAA-EO_{10}

DHAA-EO_{10} was synthesized by Zhejiang Kaider Chemical Co., Ltd., China, according to step 1 in Fig. 1.

1.2.2 Synthesis of G-DHAA-EO_{10}

As shown in step 2 of Fig. 1, DHAA-EO_{10} (7.25 g) and paraformaldehyde (0.24 g) were dissolved in 100 mL ethyl acetate in a three-necked flask. Subsequently, 15 mL sulfuric acid was slowly added to the flask under a nitrogen atmosphere. The mixture was heated to 85 ℃ and refluxed for 6 h. After the reaction was complete, the mixture was transferred to a separatory funnel, and the residual sulfuric acid was neutralized by dropwise addition of 1 mol/L sodium hydroxide solution. The ethyl acetate was removed under reduced pressure using a rotary evaporator. The crude product was purified by column chromatography (with an acetone to methanol volume ratio of 15∶1), affording the desired product in a 76% yield.



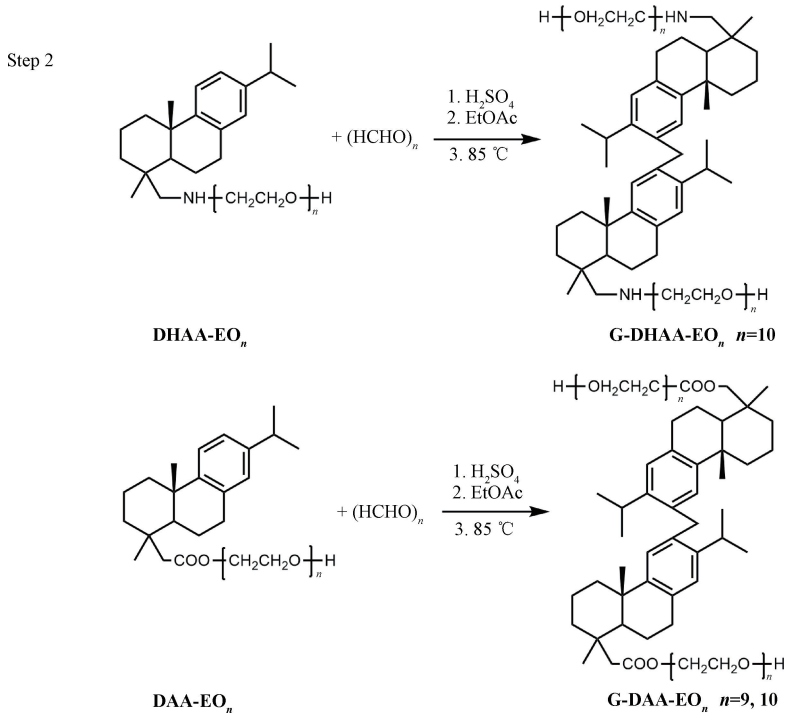


Fig. 1 Synthesis routes of G-DAA-EO$_9$, G-DAA-EO$_{10}$ and G-DHAA-EO$_{10}$

1.3 Characterization

1.3.1 Surface tension measurement

Surface tension measurements of RNGSs and OP-10 at different concentrations were performed at (25.0±0.1) ℃ using a surface tension meter (BYZ-2, Shanghai Hengping Instrument Co., Ltd., China) equipped with a platinum plate[27]. For each sample, the surface tension was measured three times, and the average value was reported.

1.3.2 Foaming property evaluation

Foaming property was evaluated by measuring the foam height. Specifically, 10 mL Gemini surfactant solutions (mass fraction of 1.0%) were placed in a 100 mL graduated cylinder and shaken vigorously by hand 50 times at (25 ± 1) ℃. The initial foam height (calculated from the volume difference between the total liquid-foam mixture and the initial 10 mL surfactant solution) was recorded immediately after shaking[28-29]. The foam height was recorded again after 5 min to evaluate foam stability. The measurement was performed three times, and the average value was reported.

1.3.3 Cloud point measurement

Cloud points of the surfactants were measured according to Ref. [30]. All samples were prepared as 1.0% (mass fraction) aqueous solutions, and their cloud points were measured using an oil bath equipped with a temperature controller. The measurement was repeated three times for each sample, and the average value was reported.

1.3.4 Dynamic light scattering measurement

The aggregation behavior of the surfactant solutions was studied by a Zetasizer (Nano-ZS, Malvern Panalytical Ltd., UK) at 25 ℃. The aqueous surfactant solutions were filtered with a 0.45 μm filter to remove the undissolved material.

1.3.5 IFT measurement

The IFT between kerosene and the RNGS was measured using the spinning drop technique with a spinning drop tensiometer (SDT, KRUSS, Germany) at 45 ℃ (the reservoir temperature of the Daqing Oilfield) and 5 000 r/min[31]. Each sample was measured three times, and the average value was reported.

1.3.6 Salt tolerance measurement

The salt tolerance of the surfactants was investigated by measuring the precipitation threshold in salt solutions with varying mass concentrations of NaCl and $CaCl_2$. The maximum salt mass concentration at which no precipitation occurs was defined as the salt tolerance.

1.3.7 Water separation rate and emulsion stability test

A 30 mL surfactant solution (mass fraction of 0.3%) was prepared and transferred to a beaker. Subsequently, 30 mL kerosene was added to the beaker. The mixture was homogenized using a homogenizer (T25, IKA, Germany) at 5 000 r/min for 3 min. The resulting emulsion was transferred to a stoppered graduated cylinder. Afterward, the graduated cylinder was placed in a water bath at 45 ℃ and allowed to stand, and the timer was started immediately. The volume of the separated water layer (lower phase) was recorded every 10 min, and the volume at time t was noted. The water separation rate S_w and emulsion stability S_{et} were calculated as

$$S_w = (V_t/V_0) \times 100\%, \quad (1)$$

$$S_{et} = (1 - V_t/V_0) \times 100\%, \quad (2)$$

where V_0 and V_t are the total volume of water added to the system and the volume at time t, respectively.

1.3.8 Static adsorption capacity measurement

The static adsorption capacity of RNGSs on quartz sand was determined by the residual mass fraction method. A 10 g portion of 100-mesh quartz sand and RNGS solution with a mass fraction of 0.3% were added to a stoppered conical flask, and the liquid-solid mass ratio was adjusted to either 5∶1 or 10∶1. The mixtures were agitated in a water bath shaker (SHZ-88A, Changzhou Henglong Instrument Co., Ltd., China) at 30 ℃ and 250 r/min for 30 h. After the mixture had clearly separated into two layers, the supernatant was collected and further centrifuged at 5 000 r/min for 20 min to remove any fine suspended particles. The adsorption amount was calculated from the difference in surfactant mass concentration before and after adsorption, as determined by potentiometric titration. The adsorption capacity η is calculated as

$$\eta = \frac{(C_1 - C_2) \times m}{M} \times 1\,000, \quad (3)$$

where C_1 is the initial mass concentration of the surfactant before adsorption; C_2 is the mass concentration of the surfactant after adsorption; m is the mass of the surfactant solution; M is the mass of the quartz sand; the factor of 1 000 converts the unit of adsorption capacity from g/g to mg/g.

2 Results and Discussion

2.1 Structure confirmation

The ^{1}H NMR spectrum of G-DHAA-EO$_{10}$ is shown in Fig. 2(a). ^{1}H NMR (400 MHz, chloroform-*d*): δ 6.93 (s, 2H, b-H), 6.67 (s, 2H, a-H), 4.30–4.10 (m, 2H, c-H), 3.84–3.36 (m, 76H, e, u-H), 3.04 (p, 4H, d, f-H), 2.74 (dd, 14H, g, h, i, j-H), 2.28–2.21 (m, 2H, k-H), 1.81–1.45 (m, 16H, n, o, l, p-H), 1.32–1.14 (m, 18H, q, r, s-H), and 0.76 (d, 6H, m-H).

The FTIR spectra of DHAA, DHAA-EO$_{10}$, and G-DHAA-EO$_{10}$ are presented in Fig. 2(b). The absorption band at 3 464.1 cm^{-1} is assigned to the stretching vibrations of —NH, which overlaps with the vibration of —OH groups. The absorption bands at 2 928.3 and 2 880.4 cm^{-1} are assigned to asymmetric and symmetric stretching vibrations of methyl and methylene groups. The peak at 1 446.2 cm^{-1} corresponds to the bending vibration of methyl groups. The peak at 1 095.1 cm^{-1} is attributed to the stretching vibration of —C—O—C—.

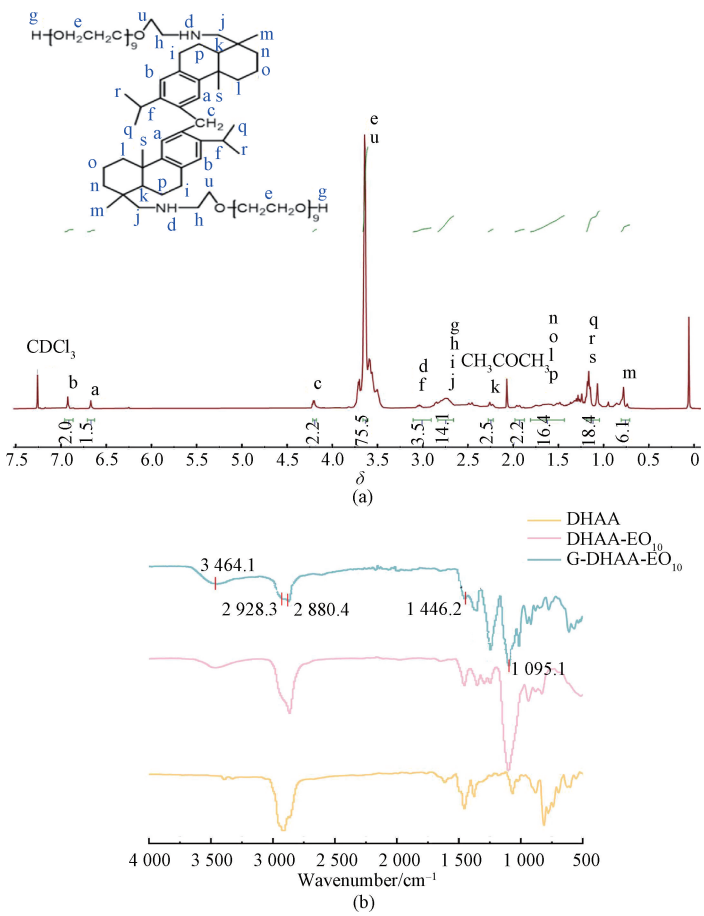


Fig. 2 Structural characterization: (a) ^{1}H NMR spectrum of G-DHAA-EO$_{10}$; (b) FTIR spectra of DHAA, DHAA-EO$_{10}$, and G-DHAA-EO$_{10}$

2.2 Surface tension

The surface tension curves of RNGSs and OP-10 as a function of the concentration are shown in Fig. 3.

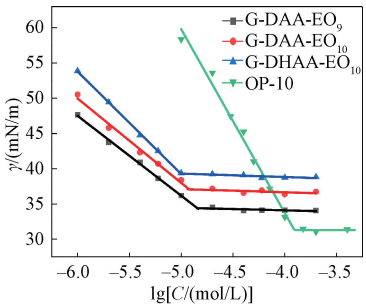


Fig. 3 Dependence of surface tension on surfactant concentration for RNGSs and OP-10

As the concentration C of surfactants increases, the surface tension γ of the solution decreases sharply and gradually levels off beyond a specific concentration threshold. The concentration at the inflection point corresponds to the CMC of the surfactant, marking the onset of micellization[32]. The CMC values of the surfactants follow the descending order: G-DAA-EO_9, G-DAA-EO_{10}, G-DHAA-EO_{10}. A comparison between G-DAA-EO_9 and G-DAA-EO_{10} reveals that the longer the hydrophilic group, the weaker the ability to reduce the surface tension. The reason is that as the degree of polymerization increases, the water solubility of G-DAA-EO_n gradually increases, and its molecules tend to dissolve in the solution, resulting in a decrease in adsorption on the surface of the solution and a weakening of the surface tension reduction performance. As the polymerization degree of EO increases, the CMC of the surfactant gradually decreases, as shown in Fig. 3. This phenomenon can be attributed to the larger number of EO units, which renders surfactant molecules more hydrophilic and more readily soluble in water[32]. With increased hydrophilicity, surfactants are less likely to accumulate at the interface and less likely to combine with water molecules to form large aggregates, making it easier to form stable micelles at lower concentrations. The lower CMC of G-DHAA-EO_{10} relative to that of G-DAA-EO_{10} can be attributed to the amine group's ability to interact with water molecules through hydrogen bonding, a property inherent to nitrogen atoms. The lone pair of electrons of the nitrogen atom is capable of forming strong hydrogen bonds with hydrogen atoms in water, which enhances the hydrophilicity of G-DHAA-EO_{10} and thus reduces the CMC of G-DHAA-EO_{10}. From the influence of polyoxyethylene chains on surface tension and CMC, it can be seen that as polyoxyethylene chains have both hydrophilicity and hydrophobicity, their impact on the surface physicochemical properties of the surfactant is comprehensive.

Moreover, surfactant molecules readily adsorb onto the air-liquid interface until surface saturation is achieved, after which micelles form in the bulk aqueous phase. The saturated adsorption capacity of the Gemini surfactant can be calculated by the Gibbs equation[33]:

$$\Gamma_{max} = -\frac{1}{2.303xRT} \times \frac{d\gamma}{d(\lg C)}, \quad (4)$$

where Γ_{max} is the saturated adsorption capacity; R is the gas constant (8.314 J/(mol · K)); T is the absolute temperature; γ is the surface tension (mN/m); C is the concentration of the surfactant; $d\gamma/d(\lg C)$ is the slope of the γ-lg$C$ curve when the concentration of the surfactant is near the CMC; x denotes the dissociation factor of the surfactant. For these new Gemini surfactants, the value of x is approximately 1. The minimum average area occupied by a single surfactant molecule A_{min} is calculated using the saturated adsorption quantity[34]:

$$A_{min} = \frac{1}{N_A \Gamma_{max}}, \quad (5)$$

where N_A is Avogadro's constant (6.022×10^{23} mol^{-1}). Another critical parameter, Π_{cmc}, is the surface pressure at the CMC, which is defined by Eq. (6)[32, 35]:

$$\Pi_{cmc} = \gamma_0 - \gamma_{cmc}, \quad (6)$$

where γ_0 and γ_{cmc} represent the surface tension of water and the surfactant solution at CMC, respectively. This parameter evaluates the effectiveness of Gemini surfactants in lowering the surface tension of water.

The above parameters obtained from Fig. 3 are listed in Table 1.

Table 1 Calculated surface activity parameters of various surfactants at 25 ℃

Surfactant	CMC/(mol/L)	γ_{cmc}/(mN/m)	$(d\gamma/d(\lg C))$/(mN/m)	Γ_{max}/(mol/m^2)	A_{min}/nm^2	Π_{cmc}/(mN/m)
G-DAA-EO_9	1.42×10^{-5}	34.42	−11.32	1.98×10^{-6}	0.838	37.58
G-DAA-EO_{10}	1.21×10^{-5}	37.07	−11.96	2.11×10^{-6}	0.787	34.93
G-DHAA-EO_{10}	8.51×10^{-6}	39.39	−15.57	2.77×10^{-6}	0.599	31.83
OP-10	1.29×10^{-4}	31.28	−26.07	4.56×10^{-6}	0.364	40.72

2.3 Foaming property

Figure 4 compares the initial foam height and foam height after 5 min for RNGSs and OP-10. In this test, the initial foam height characterizes foaming capacity, whereas the foam height measured after 5 min represents foam stability. All synthesized RNGSs exhibit inferior foaming capacity yet superior foam stability relative to OP-10. The weaker foaming capacity of RNGSs compared with OP-10 can be attributed to their poorer surface tension reduction ability, which agrees with the surface tension data in Fig. 3. A low surface tension is typically conducive to the initial formation of foam. However, an excessively low surface tension may result in the formation of a thin foam film that is susceptible to rupture, thereby reducing the foam stability[36]. Hence, the foam stability of OP-10 is worse than that of RNGSs.

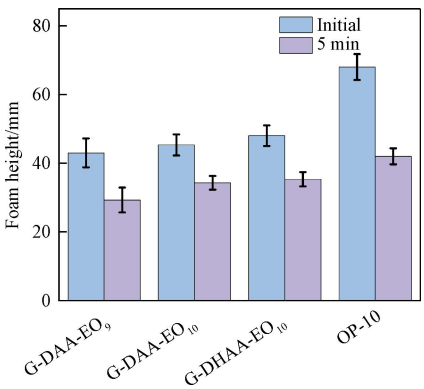


Fig. 4 Foaming property of RNGSs and OP-10

2.4 Cloud point

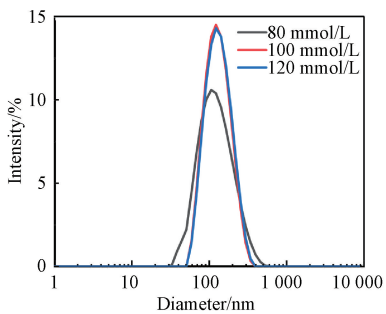
The cloud point is a key characteristic parameter of non-ionic surfactants, which partially reflects their aqueous solubility. In general, a higher cloud point corresponds to better aqueous solubility. The cloud points of RNGSs and OP-10 are shown in Table 2. It can be seen that the cloud point of G-DAA-EO_{10} is higher than that of G-DAA-EO_9. This mainly arises from the extended EO hydrophilic segment: longer polyoxyethylene chains form more hydrogen bonds with water molecules. More energy (higher temperature) is thus required to disrupt these hydrogen bonds and trigger surfactant phase separation/precipitation. Benefiting from its distinct molecular structure containing nitrogen atoms, G-DHAA-EO_{10} can form additional hydrogen bonds with water molecules upon dissolution. This extra hydrogen-bonding interaction further elevates its cloud point compared with G-DAA-EO_{10}.

Table 2 Cloud points of various surfactants

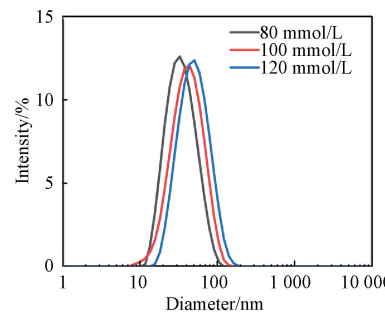
Surfactant	Cloud point/℃
G-DAA-EO_9	64.8
G-DAA-EO_{10}	70.8
G-DHAA-EO_{10}	72.6
OP-10	69.5

2.5 Size distribution of micellar aggregates

Generally, in aqueous solution, the aggregates of surfactants are formed mostly by hydrophobic interactions[37]. Figure 5 illustrates the size distribution of micellar aggregates formed by G-DAA-EO_9, G-DAA-EO_{10}, G-DHAA-EO_{10}, and OP-10 at concentrations of 80, 100, and 120 mmol/L. As illustrated in Fig. 5, the average micellar aggregate diameters of the surfactants are in the range of 100–120, 30–50, 10–15, and 10–12 nm for G-DAA-EO_9, G-DAA-EO_{10}, G-DHAA-EO_{10}, and OP-10, respectively. From Figs. 5(a) and 5(b), it can be seen that the diameter of the surfactant micellar aggregates changes with increasing concentration. Longer EO chains enhance the hydrophilicity of the surfactant. The micellar hydrophilic shell thus packs more tightly, which hinders the entanglement of hydrophobic alkyl chains and yields smaller micellar aggregate sizes. This difference originates from the Gemini molecular architecture of RNGSs. Their complex structure enables strong intermolecular forces during micellization, facilitating the assembly of surfactant monomers and promoting the formation of micellar aggregates.



(a)



(b)

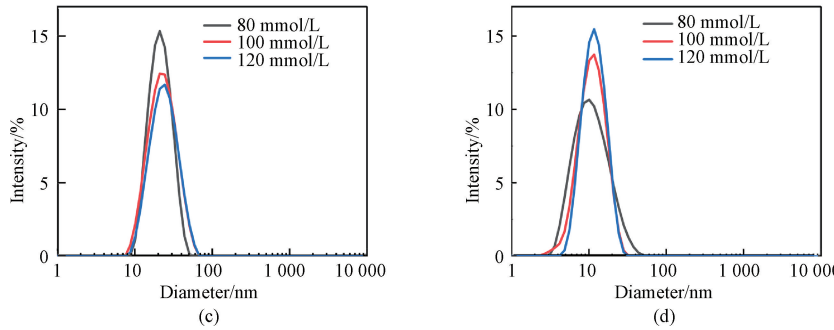


Fig. 5 Size distribution of micellar aggregates of various surfactants: (a) G-DAA-EO_9; (b) G-DAA-EO_{10}; (c) G-DHAA-EO_{10}; (d) OP-10

2.6 IFT

IFT is an important parameter for studying interfacial phenomena in liquid-liquid systems[38-40]. In the field of surfactant flooding, the IFT between oil and water is the basis for studying the interfacial properties of surfactants and the standard for screening surfactant flooding formulations. The IFT between the oil and water phases present in the reservoir is typically over 20 mN/m[41-42]. Due to such a high IFT value, oil droplets are still trapped within the narrow pores of the reservoir. Reducing the oil-water IFT enables oil droplets to readily deform and migrate through narrow capillary channels. To simulate the applicability of RNGSs in EOR under oilfield conditions, mineralized water was prepared to disperse RNGSs, and kerosene was used as the simulated crude oil.

The effects of surfactant mass concentration, NaCl mass concentration, and $CaCl_2$ mass concentration on IFT were analyzed. The variation of IFT with surfactant mass concentration is shown in Fig. 6(a). The IFT of RNGSs reaches the lowest value at a surfactant mass concentration of 3 g/L. The decrease in IFT is due to the increased adsorption of surfactants at the oil-water interface. The adsorbed surfactant molecules arrange themselves, resulting in hydrophobic carbon chains in the oil phase and hydrophilic head groups in the water phase. The interaction between carbon chains and oil components reduces IFT[43-44]. The lowest value of IFT is attained when the surfactant molecules reach saturated adsorption at the oil-water interface; any further increase in the surfactant mass concentration cannot reduce the oil-water IFT. In aqueous solution, the EO chains of both G-DHAA-EO_{10} and OP-10 undergo entanglement. However, due to the distinctive structural characteristics of G-DHAA-EO_{10}, its distribution at the oil-water interface is less uniform than that of OP-10. Consequently, the IFT of G-DHAA-EO_{10} at the oil-water interface is higher than that of OP-10.

Figure 6 (b) shows the variation of IFT with the mass concentration of NaCl. The results indicate that the equilibrium IFT of each system first decreases and reaches the lowest value, and then increases with increasing NaCl mass concentration. For RNGSs, the lowest IFT is attained at the NaCl mass concentration of 30 g/L. The salinity at which the IFT value is the lowest is called the optimum salinity of the system, which is related to its oil affinity. A comparison between G-DAA-EO_9 and G-DAA-EO_{10} shows that with the increase of EO groups, the solubility of surfactants is enhanced while the lipophilicity is weakened, and a lower IFT can be obtained in a range of higher salinity. G-DHAA-EO_{10} possesses stronger hydrophilicity than G-DAA-EO_{10}, so it delivers more efficient IFT reduction at identical NaCl mass concentrations. RNGSs exhibit better NaCl resistance than OP-10, as can be seen in Fig. 6 (b). The oil-water IFT of OP-10 is about 1 mN/m lower than that of RNGSs in the NaCl system.

The lowest IFT occurs at optimal salinity, where surfactant partitioning between water and oil is balanced. IFT depends on aqueous-phase salt content, which governs surfactant solubility. NaCl exhibits two competing effects on IFT. At low NaCl mass concentrations, most surfactant molecules dissolve exclusively in the aqueous phase, leading to low interfacial adsorption and relatively high IFT. As NaCl mass concentration rises, the electric double layer at the oil-water interface is compressed; the electrostatic repulsion between surfactant head groups declines, allowing tighter molecular packing and a corresponding reduction in IFT. At high NaCl mass concentrations, salting-out drives surfactant molecules into the oil phase, decreasing interfacial coverage and increasing IFT. At intermediate NaCl mass concentrations, surfactant distributes equally between water and oil phases, establishing a balanced interfacial state that yields the lowest IFT. This moderate NaCl mass concentration is referred to as the optimal salinity.

To assess the divalent salt tolerance of RNGSs, the oil-water IFT of RNGS was measured at different $CaCl_2$ mass concentrations. The results are shown in Fig. 6(c). The IFT gradually declines with increasing $CaCl_2$ mass concentrations, reaching the lowest value at 8 g/L, and subsequently increases. This trend mirrors that observed with NaCl, where low salinity enhances surfactant interfacial activity, while high salinity suppresses it. At low $CaCl_2$ mass concentrations, increased salinity

promotes surfactant partitioning into the oil phase, enhancing interfacial adsorption and reducing IFT. At high mass concentrations, excessive Ca^{2+} weakens surfactant hydration via interaction with water oxygen atoms, reducing solubility and stability, and partially shielding hydrophilic groups, thereby increasing IFT.

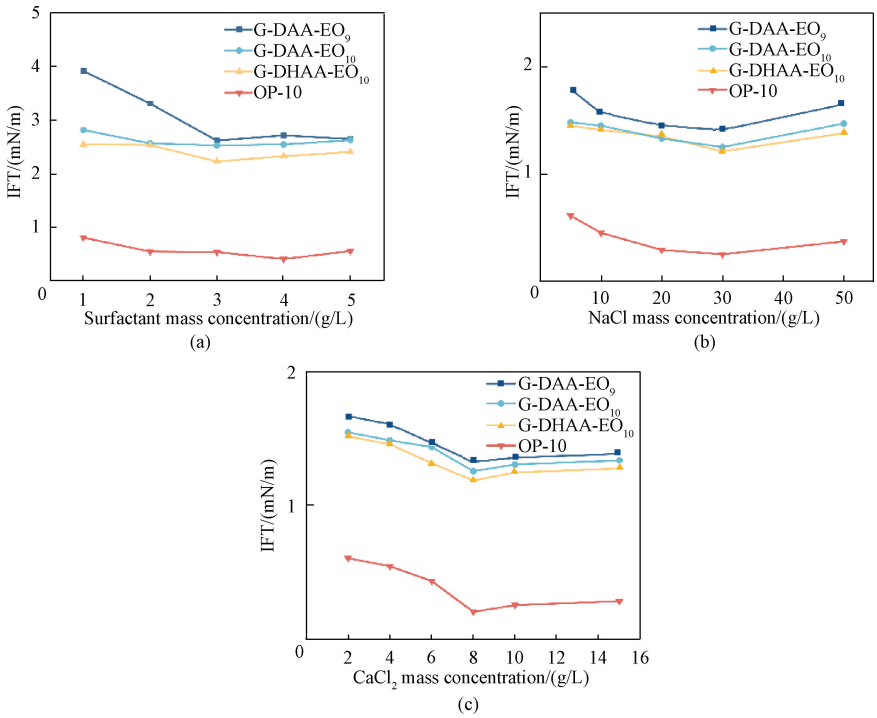


Fig. 6 IFT between kerosene and water under different conditions: (a) different surfactant mass concentrations; (b) different NaCl mass concentrations; (c) different $CaCl_2$ mass concentrations

2.7 Salt tolerance

The salt tolerance of surfactants is an important indicator for evaluating the feasibility of their application in high-salinity oil reservoirs[45-46]. Surfactants with poor salt tolerance will precipitate in high-salinity formations, which reduces the oil recovery factor. Tables 3 and 4 summarize the aqueous solubility of RNGSs in NaCl and $CaCl_2$ solutions at varying mass concentrations, with corresponding visual photographs presented in Figs. 7 and 8. The mass concentration of NaCl ranges from 5 to 310 g/L, while the mass concentration of $CaCl_2$ ranges from 0.2 to 10.0 g/L. As shown in Table 3, the salt tolerance of G-DAA-EO_n improves as the number of EO groups increases. No precipitation appears in the G-DHAA-EO_{10} system when the NaCl mass concentration is 300 g/L. In contrast, new phases form in G-DAA-EO_9, G-DAA-EO_{10}, and OP-10 solutions at NaCl concentrations of 100, 140, and 150 g/L, respectively. For G-DAA-EO_n surfactants with fixed hydrophobic carbon chain length, molecular hydrophilicity rises with longer EO chains. More hydrogen bonds can be formed between water molecules and hydrophilic head groups, making it difficult to form precipitates in saline solutions. G-DHAA-EO_{10} forms a greater number of hydrogen bonds in aqueous solutions than G-DAA-EO_{10}. Consequently, G-DHAA-EO_{10} exhibits superior salt tolerance compared with G-DAA-EO_{10}. As shown in Table 4, none of the test samples generate precipitates at $CaCl_2$ mass concentrations up to 10.0 g/L. The salt tolerance of G-DHAA-EO_{10} is superior to that of previously reported oil-displacement surfactants[23-26]. For example, the zwitterionic Gemini surfactant synthesized by Liu et al.[23] exhibited salt tolerance of 160 g/L for NaCl and 10 g/L for $CaCl_2$. Overall, these results demonstrate that the synthesized surfactants possess outstanding salt tolerance and are promising candidates for applications in high-salinity oil reservoirs[44].

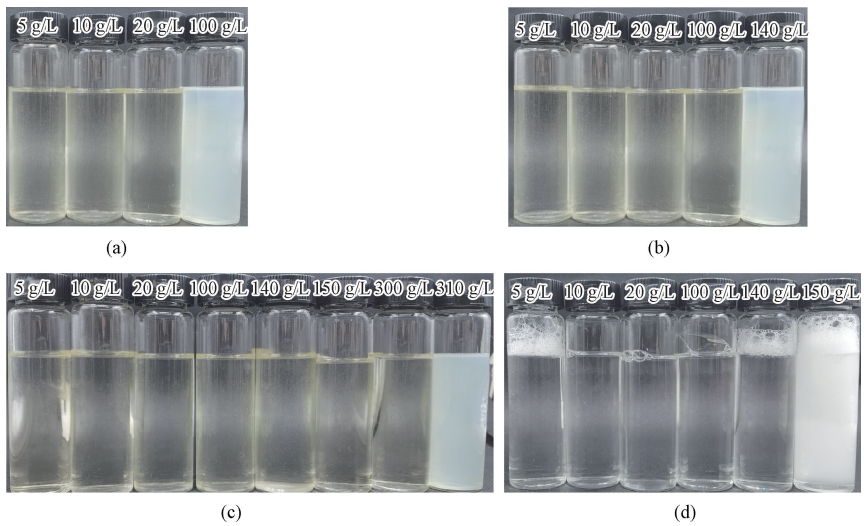
Table 3 Effects of NaCl mass concentration on aqueous stability of RNGSs and OP-10

Surfactant	Mass concentration of NaCl/(g/L)							
	5	10	20	100	140	150	300	310
G-DAA-EO_9	−	−	−	+	+	+	+	+
G-DAA-EO_{10}	−	−	−	−	+	+	+	+
G-DHAA-EO_{10}	−	−	−	−	−	−	−	+
OP-10	−	−	−	−	−	+	+	+

Notes: − means a clear and homogeneous solution without phase separation or precipitate; + means a new phase appears in the solution.

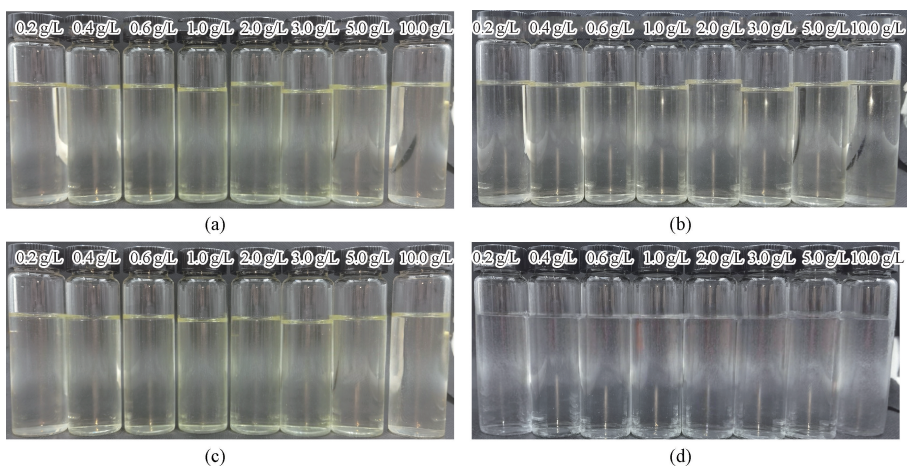
Table 4 Effects of $CaCl_2$ mass concentration on aqueous stability of RNGSs and OP-10

Surfactant	Mass concentration of $CaCl_2$/(g/L)							
	0.2	0.4	0.6	1.0	2.0	3.0	5.0	10.0
G-DAA-EO_9	−	−	−	−	−	−	−	−
G-DAA-EO_{10}	−	−	−	−	−	−	−	−
G-DHAA-EO_{10}	−	−	−	−	−	−	−	−
OP-10	−	−	−	−	−	−	−	−



(a) (b) (c) (d)

Fig. 7 Visual photographs of saline solutions containing different surfactants at different NaCl mass concentrations: (a) G-DAA-EO_9; (b) G-DAA-EO_{10}; (c) G-DHAA-EO_{10}; (d) OP-10



(a) (b) (c) (d)

Fig. 8 Visual photographs of saline solutions containing different surfactants at different $CaCl_2$ mass concentrations: (a) G-DAA-EO_9; (b) G-DAA-EO_{10}; (c) G-DHAA-EO_{10}; (d) OP-10

2.8 Water separation rate and emulsion stability

The oil displacement mechanism of surfactants indicates that their emulsifying properties have a significant impact on oil displacement efficiency. Therefore, in addition to the low IFT and good wettability, evaluating the emulsifying performance of surfactants is essential for improving crude oil recovery.

The water separation rate method was used to evaluate the emulsifying performance of the surfactants. In terms of the water separation rate shown in Fig. 9(a), G-DAA-EO_9 presents the highest value, followed by G-DAA-EO_{10}, and G-DHAA-EO_{10} has a comparable water separation rate to OP-10, where a higher water separation rate corresponds to lower emulsion stability. With regard to emulsion stability displayed in Fig. 9(b), OP-10 and G-DHAA-EO_{10} exhibit approximately similar stability performance, G-DAA-EO_{10} ranks the second, and G-DAA-EO_9 delivers the weakest emulsion stability.

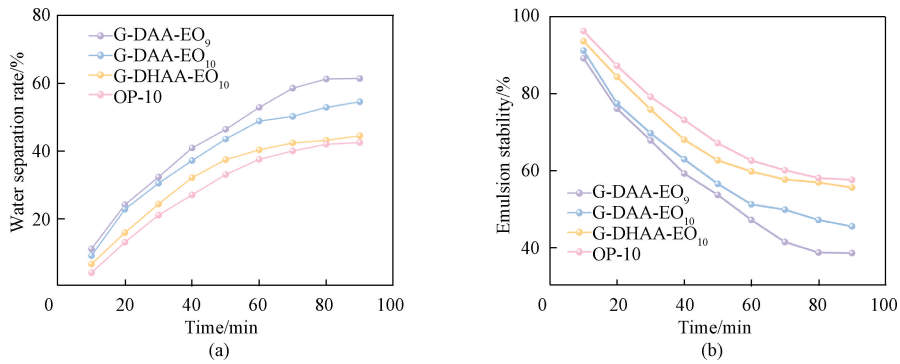


Fig. 9 Emulsifying performance of RNGSs and OP-10: (a) water separation rate; (b) emulsion stability

2.9 Static adsorption capacity

When surfactants are injected into underground reservoirs, their adsorption loss onto porous media during oil recovery impairs the oil recovery factor. This phenomenon not only raises production costs but also restricts the practical application of surfactants for EOR[47-48]. In this experiment, the adsorption capacity of RNGSs on quartz sand was studied. The results are shown in Fig. 10.

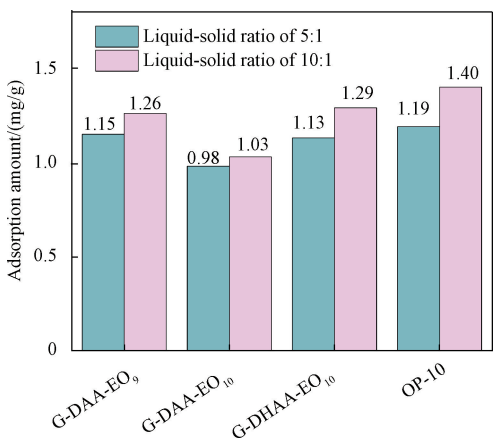


Fig. 10 Adsorption amount of RNGSs and OP-10 versus liquid-solid ratio

The results indicate that as the liquid-solid ratio increases, the adsorption capacity of RNGSs on quartz sand increases. This adsorption behavior can be interpreted as the partitioning equilibrium of adsorbate molecules between the solid-liquid interface and bulk aqueous solution. For G-DAA-EO_9 and G-DAA-EO_{10}, their equilibrium adsorption amounts onto quartz sand are different, which means that the number of EO groups in the molecular chain exerts an influence on adsorption capacity. A comparison between G-DHAA-EO_{10} and G-DAA-EO_{10} shows that molecular hydrophilicity regulates their adsorption amount onto quartz sand; the more hydrophilic G-DHAA-EO_{10} exhibits higher adsorption capacity at the same liquid-solid ratio.

3 Conclusions

Novel rosin-based non-ionic Gemini surfactants were synthesized from rosin derivatives, DAA and DHAA. Measurements of CMC, foam stability, and cloud point demonstrate that the synthesized surfactants exhibit superior comprehensive performance compared with the commercial non-ionic surfactant OP-10. The potential of the synthesized surfactants for EOR applications was verified by IFT, static adsorption capacity, salt tolerance, water separation rate, and emulsion stability tests. This research provides an effective strategy to elevate the economic added value of rosin resources. Future research will expand the application scope of such rosin-based Gemini surfactants and focus on the design and synthesis of rosin-derived cationic and anionic Gemini surfactants.

References

[1] Zhang W J, Ye S F, Zhai Z L, et al. Preparation and application of wormlike micelles generated from a rosin-based aggregation-induced emission surfactant through coordinating aggregation[J]. *Journal of Molecular Liquids*, 2024, 410: 125623.

[2] Mantzaridis C, Brocas A L, Llevot A, et al. Rosin acid oligomers as precursors of DGEBA-free epoxy resins[J]. *Green Chemistry*, 2013, 15(11): 3091-3098.
[3] Liang T B, Zhao X R, Yuan S, et al. Surfactant-EOR in tight oil reservoirs: current status and a systematic surfactant screening method with field experiments[J]. *Journal of Petroleum Science and Engineering*, 2021, 196: 108097.
[4] Yu J, Xu C Q, Song X L, et al. Synthesis and properties of rosin grafted polymers via "grafting from" ATRP: the role of rosin-based initiator [J]. *Industrial Crops and Products*, 2021, 168: 113610.
[5] Zhai Z L, Yan X Y, Song Z Q, et al. Annular and threadlike wormlike micelles formed by a bio-based surfactant containing an extremely large hydrophobic group[J]. *Soft Matter*, 2018, 14 (4): 499-507.
[6] Zhao Y Z, Zhou J Y, Lei F H, et al. Temperature induced multiple structure transformation and aggregation behaviors of amphiphilic acrylicpimaric acid polyglycol ester in water[J]. *Polymer*, 2017, 118: 49-57.
[7] Zhu X F, Zhang J, Zhou J Y, et al. Adsorption characteristics and conformational transition of polyethylene glycol-maleated rosin polyesters on the water-air surface[J]. *Advanced Composites and Hybrid Materials*, 2022, 5(2): 1233-1240.
[8] Pal N, Saxena N, Mandal A. Studies on the physicochemical properties of synthesized tailor-made gemini surfactants for application in enhanced oil recovery[J]. *Journal of Molecular Liquids*, 2018, 258: 211-224.
[9] Lei L, Xie D H, Song B L, et al. Photoresponsive foams generated by a rigid surfactant derived from dehydroabietic acid[J]. *Langmuir*, 2017, 33(32): 7908-7916.
[10] Liu D T, Yang X, Liu P, et al. Synthesis and characterization of gemini ester surfactant and its application in efficient fabric softening [J]. *Journal of Molecular Liquids*, 2020, 299: 112236.
[11] Zhao W W, Wang Y L. Coacervation with surfactants: from single-chain surfactants to gemini surfactants[J]. *Advances in Colloid and Interface Science*, 2017, 239: 199-212.
[12] Al-Azani K, Abu-Khamsin S, Kamal M S, et al. Role of injection rate on chemically enhanced oil recovery using a gemini surfactant under harsh conditions [J]. *Energy & Fuels*, 2024, 38(5): 3682-3692.
[13] Deng X, Kamal M S, Patil S, et al. Wettability alteration on carbonate rock by the mixture of the gemini surfactant and chelating agent [J]. *Energy & Fuels*, 2022, 36(22): 13652-13664.
[14] Yao Y, Fu Y F, Zhang L, et al. Synthesis, properties, and applications of an anionic-nonionic Gemini surfactant for highly efficient remediation of perchloroethylene-contaminated aquifers [J]. *Journal of Cleaner Production*, 2022, 333: 130143.
[15] Tan W X, Lin Z T, Bu H T, et al. Nano-micelles based on a rosin derivative as potent sorbents and sinking agents with high absorption capabilities for the removal of metal ions [J]. *RSC Advances*, 2012, 2(18): 7279-7289.
[16] Pan Y Q, Ge B Q, Zhang Y L, et al. Surface activity and cleaning performance of Gemini surfactants with rosin groups [J]. *Journal of Molecular Liquids*, 2021, 336: 116222.
[17] Xu Y R, Niu Y F, Wu C H, et al. Synthesis, characterization, antifungal properties of quaternary ammonium salts derived from natural rosin[J]. *Biomass Conversion and Biorefinery*, 2024, 14(16): 18803-18811.
[18] Yan X Y, Zhai Z L, Song Z Q, et al. Synthesis and properties of polyester-based polymeric surfactants from diterpenic rosin[J]. *Industrial Crops and Products*, 2017, 108: 371-378.
[19] Wang M G, Yang X F, Han B, et al. Design and properties of natural rosin-based phosphoester functional surfactants[J]. *Molecules*, 2023, 28 (7): 3091.
[20] Deng W X, Zhang Y C, Zhong Y W, et al. Synthesis and thermodynamic properties of rosin-based cationic gemini surfactants[J]. *Journal of Surfactants and Detergents*, 2014, 17(3): 453-458.
[21] Feng L, Xie D H, Song B L, et al. Aggregate evolution in aqueous solutions of a Gemini surfactant derived from dehydroabietic acid[J]. *Soft Matter*, 2018, 14(7): 1210-1218.
[22] Feng H Y, Pan Y Q, Zhang Y J, et al. Surface activity and cleaning performance of rosin-based quaternary ammonium salt type asymmetric Gemini surfactants [J]. *Chinese Journal of Chemical Engineering*, 2024, 73: 70-80.
[23] Liu J H, Liu Z, Yuan T J, et al. Synthesis and properties of zwitterionic gemini surfactants for enhancing oil recovery[J]. *Journal of Molecular Liquids*, 2020, 311: 113179.
[24] Bao X N, Li Y C, Zhang W D, et al. A new thermal stable and salt tolerant alkyl polyether benzyl sulfonate surfactant with ultralow interfacial tensions for enhanced oil recovery[J]. *Energy & Fuels*, 2023, 37(3): 1828-1835.
[25] Cheng Y Q, Xue L N, Niu C R, et al. Synthesis and properties of a novel asymmetric gemini surfactant based on siloxane skeleton[J]. *Journal of Molecular Liquids*, 2019, 296: 112073.
[26] Kumar S, Saxena N, Mandal A. Synthesis and evaluation of physicochemical properties of anionic polymeric surfactant derived from Jatropha oil for application in enhanced oil

recovery [J]. *Journal of Industrial and Engineering Chemistry*, 2016, 43: 106-116.
[27] Zhao W H, Cheng Y Q, Lu S, et al. Synthesis and surface activity of two novel phosphate silicone surfactants [J]. *Journal of Molecular Liquids*, 2023, 390: 123154.
[28] Li P, Guo Y X, Lu Z, et al. Syntheses, surface activities and aggregation morphologies of a series of novel itaconic acid based asymmetrical gemini surfactants [J]. *Journal of Molecular Liquids*, 2019, 290: 111218.
[29] Su S K, Lin L H, Lai Y C. Surface activity and cleavability of gemini surfactants featuring hydrophilic spacer groups [J]. *Journal of Surfactants and Detergents*, 2012, 15(6): 745-750.
[30] Dong Q W, Li X, Dong J X. Synthesis and properties of ethoxylated vicinal diol nonionic surfactants with double hydrophilic head groups [J]. *Colloids and Surfaces A: Physicochemical and Engineering Aspects*, 2022, 634: 127971.
[31] Chen S Y, Liu H J, Sun H, et al. Synthesis and physiochemical performance evaluation of novel sulphobetaine zwitterionic surfactants from lignin for enhanced oil recovery [J]. *Journal of Molecular Liquids*, 2018, 249: 73-82.
[32] Man Z Q, Wu W X. Study on the synthesis, surface activity, and self-assembly behavior of anionic non-ionic gemini surfactants [J]. *Molecules*, 2024, 29(8): 1725.
[33] Yang C P, Song Z Z, Zhao J J, et al. Self-assembly properties of ultra-long-chain gemini surfactants bearing multiple amide groups with high performance in fracturing fluid application [J]. *Colloids and Surfaces A: Physicochemical and Engineering Aspects*, 2017, 523: 62-70.
[34] Cai B, Li X F, Yang Y, et al. Surface properties of Gemini surfactants with pyrrolidinium head groups [J]. *Journal of Colloid and Interface Science*, 2012, 370(1): 111-116.
[35] Cheng Y M, Liu X, Lei Q F, et al. Development of novel anionic Gemini surfactants and application in fabricating hierarchical silver microparticles for surface-enhanced Raman spectroscopy [J]. *Journal of Colloid and Interface Science*, 2017, 505: 1074-1081.
[36] Xie Y C, Li J, Zhu R H, et al. Synthesis, surface activity, thermodynamic parameters, and performance evaluation of branched carboxylate gemini surfactants [J]. *Journal of Surfactants and Detergents*, 2019, 22(3): 421-430.
[37] Tan J L, Xiao M H, Hu Q H. Aggregation behavior of "linear" trisiloxane surfactant with different terminal groups (CH_3—, $ClCH_2$—, and CF_3—) in aqueous solution [J]. *The Journal of Physical Chemistry B*, 2019, 123(16): 3543-3549.
[38] Ma B D, Gao B Y, Zhang L, et al. Influence of polymer on dynamic interfacial tensions of EOR surfactant solutions [J]. *Journal of Applied Polymer Science*, 2014, 131(15): 40562.
[39] Liu Z L, Zhao G, Brewer M, et al. Comprehensive review on surfactant adsorption on mineral surfaces in chemical enhanced oil recovery [J]. *Advances in Colloid and Interface Science*, 2021, 294: 102467.
[40] Atta D Y, Negash B M, Yekeen N, et al. A state-of-the-art review on the application of natural surfactants in enhanced oil recovery [J]. *Journal of Molecular Liquids*, 2021, 321: 114888.
[41] Lashkarbolooki M, Ayatollahi S, Riazi M. The impacts of aqueous ions on interfacial tension and wettability of an asphaltenic-acidic crude oil reservoir during smart water injection [J]. *Journal of Chemical & Engineering Data*, 2014, 59(11): 3624-3634.
[42] Sakthivel S, Gardas R L, Sangwai J S. Effect of alkyl ammonium ionic liquids on the interfacial tension of the crude oil-water system and their use for the enhanced oil recovery using ionic liquid-polymer flooding [J]. *Energy & Fuels*, 2016, 30(3): 2514-2523.
[43] Rostami A, Hashemi A, Ali Takassi M, et al. Experimental assessment of a lysine derivative surfactant for enhanced oil recovery in carbonate rocks: mechanistic and core displacement analysis [J]. *Journal of Molecular Liquids*, 2017, 232: 310-318.
[44] Guo J X, Shi X, Yang Z G, et al. Synthesis of temperature-resistant and salt-tolerant surfactant SDB-7 and its performance evaluation for Tahe Oilfield flooding (China) [J]. *Petroleum Science*, 2014, 11(4): 584-589.
[45] Sharifi A, Miri R, Riazi M. A holistic review of harsh conditions resistant surfactants for enhanced oil recovery in dense carbonate reservoir [J]. *Fuel*, 2023, 353: 129109.
[46] Afolabi F, Mahmood S M, Yekeen N, et al. Polymeric surfactants for enhanced oil recovery: a review of recent progress [J]. *Journal of Petroleum Science and Engineering*, 2022, 208: 109358.
[47] Kalam S, Abu-Khamsin S A, Patil S, et al. Adsorption reduction of a gemini surfactant on carbonate rocks using formic acid: static and dynamic conditions [J]. *Fuel*, 2023, 345: 128166.
[48] Jian G Q, Puerto M, Wehowsky A, et al. Characterizing adsorption of associating surfactants on carbonates surfaces [J]. *Journal of Colloid and Interface Science*, 2018, 513: 684-692.

松香基聚氧乙烯醚非离子型双子表面活性剂的合成与应用

韩召强[1]，张瑞峰[1]，张　瑞[1]，王碧佳[1]，纪柏林[1]，徐　红[1]，毛志平[1,2*]，钟　毅[1,3*]

1. 东华大学 绿色低碳纺织印染技术教育部重点实验室，化学与化工学院，纺织科学与技术创新中心，上海 201620
2. 国家先进印染技术创新中心，山东中康国创先进印染技术研究院有限公司，山东 泰安 271000
3. 塔里木大学 纺织服装学院，现代纺织材料与技术兵团重点实验室，新疆 阿拉尔 843300

摘　要：本研究以松香衍生物——脱氢松香酸和脱氢松香胺为原料，通过加成和烷基化反应，合成了新型松香基非离子型双子表面活性剂（rosin-based nonionic Gemini surfactant，RNGS）。采用傅里叶变换红外光谱和核磁共振氢谱对所合成表面活性剂的结构进行了表征。利用表面张力测试和动态光散射技术，研究了RNGS 在水溶液中的表面活性、聚集行为和发泡性能。同时，测定了其浊点，以评估表面活性剂的最高适用温度。为考察 RNGS 在提高原油采收率方面的应用潜能，对其界面张力、静态吸附量、耐盐性和乳化稳定性进行了研究。RNGS 的临界胶束浓度（critical micelle concentration，CMC）为 8.51×10^{-6} mol/L，低于常用的非离子表面活性剂 OP-10 的 CMC（1.29×10^{-4} mol/L）。RNGS 的浊点可达 72.6 ℃。此外，该表面活性剂对 NaCl 和 $CaCl_2$ 的耐受质量浓度分别可达 300 g/L 和 10 g/L。上述研究结果表明，所合成的表面活性剂在提升原油采收率方面具有潜在的应用前景。

关键词：非离子型双子表面活性剂；松香衍生物；提升原油采收率